Nitroxide Scanning Electron Paramagnetic Resonance of Helices IV and V and the Intervening Loop in the Lactose Permease of *Escherichia coli*†

Min Zhao,‡ Kuo-Chang Zen,‡ Jordi Hernandez-Borrell,‡ Christian Altenbach,§ Wayne L. Hubbell,§ and H. Ronald Kaback*,‡

Howard Hughes Medical Institute, Departments of Physiology and Microbiology & Molecular Genetics, and Jules Stein Eye Institute and Department of Chemistry & Biochemistry, University of California at Los Angeles, Los Angeles, California 90095-1662

Received July 28, 1999; Revised Manuscript Received September 22, 1999

ABSTRACT: Glu126 and Arg144 in helices IV and V, respectively, in the lactose permease of *Escherichia coli*, which play an indispensable role in substrate binding, are charge-paired and in close proximity [Venkatesan, P., Kaback, H. R. (1998) *Proc. Natl. Acad. Sci. U.S.A. 95*, 9802−9807; Zhao, M., Zen, K.-C., et al. (1999) *Biochemistry 38*, 7407−7412]. Since hydropathy plots indicate that these residues are at the membrane−water interface at the cytoplasmic surface of the membrane, site-directed nitroxide scanning electron paramagnetic resonance (EPR) has been carried out on this region of the permease. Thirty-one single-Cys permease mutants were spin-labeled and examined by conventional and power saturation EPR. The motional freedom of the side chains, as well as accessibility to O_2 or potassium chromium oxalate (CrOx), indicates that the loop between helices IV and V (loop IV/V) is considerably smaller than predicted by hydropathy plots, extending only from about Val132 to Phe138 and that Glu126 and Arg144 are probably within the membrane. Although ligand binding has no effect on the mobility of the labeled side chains, a marked increase in CrOx and O_2 accessibility is observed at position 137, as well as significant changes in accessibility to CrOx on one face of helix V. It is concluded that ligand binding induces a conformational change in the vicinity of the binding site, resulting in increased accessibility of position 137 in loop IV/V to solvent.

The lactose permease (lac permease)[1] of *Escherichia coli* is representative of secondary active transport proteins that convert free energy stored in electrochemical ion gradients into work in the form of a concentration gradient. This hydrophobic, polytopic cytoplasmic membrane protein encoded by the *lacY* gene of the *lac* operon (*1*) catalyzes the coupled stoichiometric translocation of galactosides with H^+ (reviewed in refs *2*−*4*). The permease has been solubilized from the membrane, purified, reconstituted into proteoliposomes in a fully functional state (reviewed in ref *5*), and shown to be solely responsible for β-galactoside transport as a monomer (see ref *6*). All available evidence indicates that the permease consists of 12 transmembrane α-helices connected by hydrophilic loops with the N and C termini on the cytoplasmic face of the membrane (reviewed in refs *7* and *8*) (Figure 1).

Site-directed mutagenesis of wild-type permease and Cys-scanning mutagenesis of a functional mutant devoid of Cys residues (C-less permease) reveals that only six out of 417 residues in the protein are irreplaceable with respect to active transport (reviewed in refs *9* and *10*). Glu269 (helix VIII), Arg302 (helix IX), His322 (helix X), and Glu325 (helix X) play critical roles in H^+ translocation and coupling, while Glu126 (helix IV) and Arg144 (helix V), which were among the last residues to be mutated (*11*), are major determinants for substrate binding (*12*, *13*). Moreover, replacement of either Glu126 or Arg144 with Ala markedly decreases the reactivity of Cys148, a residue that interacts weakly and hydrophobically with the galactosyl moiety of the substrate (*14*, *15*). In contrast, interchanging the residues, double-Ala replacement, or replacement of Arg144 with Lys or His has little or no effect on Cys148 reactivity, thereby indicating that Glu126 and Arg144 are charge-paired and therefore likely to be in a relatively low dielectric environment (*12*). In addition, permease mutant E126H/R144H[2] binds Mn(II) with high affinity in a pH-dependent fashion, and the appropriately labeled double-Cys mutant exhibits excimer fluorescence or spin−spin interactions, demonstrating that

† This work was supported in part by NIH Grant DK1131 to H.R.K. and by a Jules Stein Professorship Endowment to W.L.H. J.H.-B. was supported by a fellowship from the GP Catalonian Studies Program.

* To whom correspondence should be addressed.

‡ HHMI, Departments of Physiology and Microbiology & Molecular Genetics.

§ Jules Stein Eye Institutes and Department of Chemistry & Biochemistry.

[1] Abbreviations: lac permease, lactose permease; Cys-less permease, functional lactose permease devoid of Cys residues; SDSL, site-directed spin labeling; EPR, electron paramagnetic resonance; DPPH, 2,2-diphenyl-1-picrylhydrazyl; $NaDodSO_4$, sodium dodecyl sulfate; PCR, polymerase chain reaction; DM, *n*-dodecyl β-D-maltopyranoside; OG, octyl β-D-glucopyranoside; TDG, β-D-galactopyranosyl 1-thio-β-D-galactopyranoside; CrOx, potassium chromium oxalate (potassium trioxalatochromate); DTT, dithiothreitol; KP_i, potassium phosphate.

[2] Site-directed mutants are designated by the single-letter amino acid abbreviation for the targeted residue, followed by the sequence position of the residue in the wild-type lac permease, and followed by a second letter indicating the amino acid replacement.

10.1021/bi991754x CCC: $18.00
Published on Web 11/09/1999

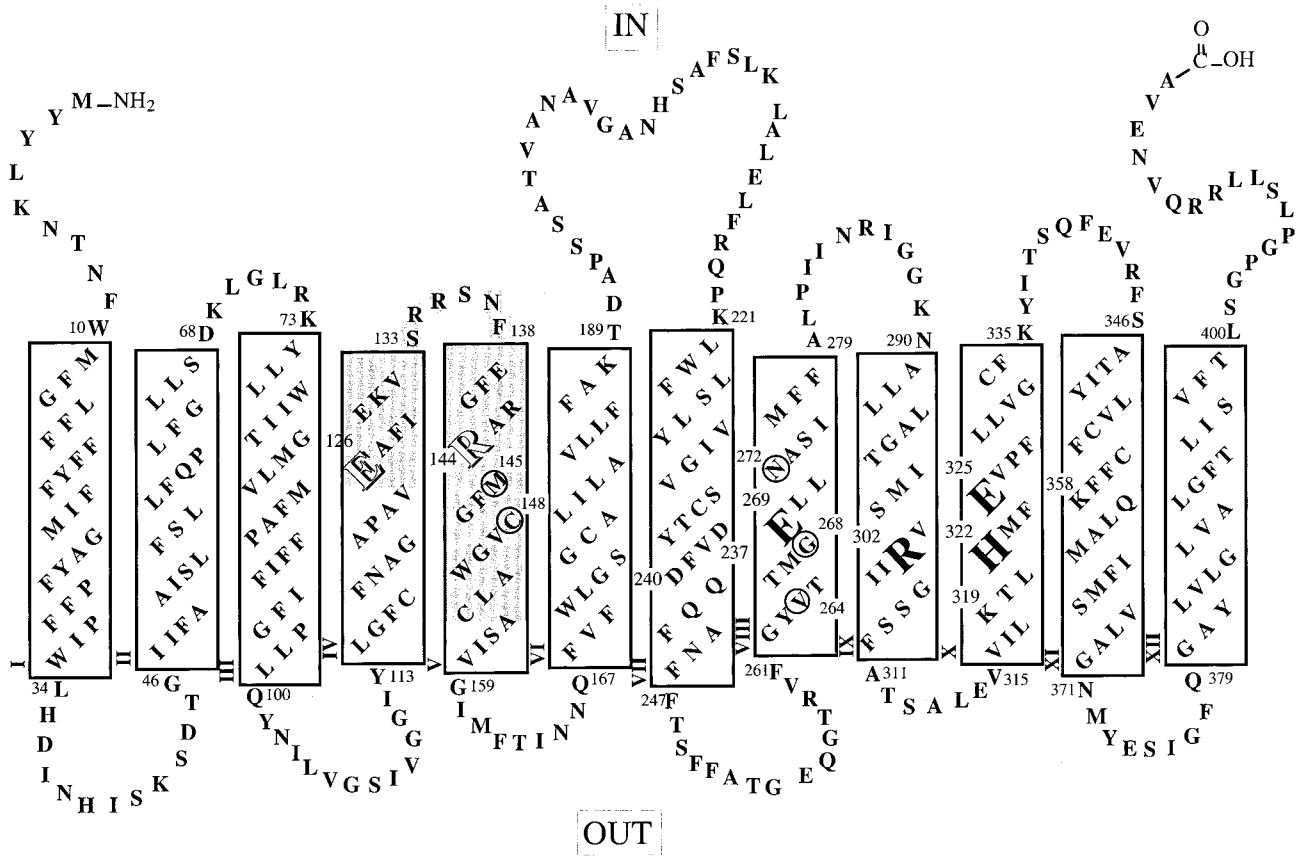

FIGURE 1: Secondary structure of lac permease, as modified by Wolin and Kaback (*18*), showing regions subjected to nitroxide-scanning EPR. The one-letter amino acid code is used, and putative transmembrane helices are shown in boxes. Residues irreplaceable with respect to active transport are enlarged: those involved in substrate translocation are shown as open letters [Glu-126 (helix IV) and Arg-144 (helix V)], and those involved in H^+ translocation and coupling are shown in black [Glu-269 (helix VIII), Arg-302 (helix IX), His-322 (helix X), and Glu-325 (helix X)]. Asp-237 (helix VII) and Lys-358 (helix XI), as well as Asp-240 (helix VII) and Lys-319 (helix X), which are charge-paired, are numbered. Nonessential residues thought to be involved in substrate translocation [Met-145 and Cys-148 (helix V), and Val-264, Gly-268, and Asn-272 (helix VIII)] are encircled. The region studied here is shaded.

positions 126 and 144 are in close proximity (*16*). Although Glu126 and Arg144 were initially placed at the membrane−water interface at the cytoplasmic ends of helices IV and V, respectively (*17*), amino acid deletion analysis (*18*) and lac permease fusions with the NG domain of *FtsY* (E. Bibi, personal communication) indicate that both residues are embedded in the membrane, probably about two helical turns from the cytoplasmic ends of helices IV and V.

Site-directed spin labeling (SDSL) is a powerful tool for investigating topography, secondary structure, tertiary structure, interresidue distances, and dynamics of membrane proteins (for general reviews, see refs *19*−*22*). In this study, permease mutants with a single-Cys residue at positions 126−156 were derivatized with a thiol-specific nitroxide spin label and studied by conventional electron paramagnetic resonance (EPR) to reveal side-chain dynamics, as well as power saturation EPR to reveal local environmental features in terms of solvent accessibility. Taken together, the results indicate that the loop IV/V is much smaller than predicted, extending from Val132 to Phe138. Furthermore, results are presented indicating that ligand-binding induces conformational changes in this region of the permease.

EXPERIMENTAL PROCEDURES

Materials

(1-Oxyl-2,2,5,5-tetramethylpyrroline-3-methyl)methanethiosulfonate (methanethiosulfonate spin label) was purchased from Toronto Scientific, Inc. (Toronto, Canada). Deoxyoligonucleotides were synthesized on an Applied Biosystems 391 DNA synthesizer. All restriction endonucleases and T4 DNA ligase were from New England Biolabs (Beverly, MA). Sequenase enzyme was purchased from U.S. Biochemical Corp. (Cleveland, OH). All other materials were reagent-grade and were obtained from commercial sources.

Methods

Construction, Expression, and Purification of Lac Permease Mutants. Construction of the single-Cys mutants used in this study was described previously (*23*, *24*). To facilitate purification, the biotin acceptor domain from a *Klebsiella pneumoniae* oxaloacetate decarboxylase was inserted into loop VI/VII or at the C-terminus (*25*). The desired mutations were confirmed by using dideoxynucleotide sequence analysis (*26*, *27*). *E. coli* T184 (*lacZ*$^-$*Y*$^-$) transformed with plasmid encoding a given mutant was grown aerobically at 37 °C in Luria−Bertani broth with streptomycin (10 μg/mL) and ampicillin (100 μg/mL). Fully grown cultures were diluted 10-fold in a 12 L fermenter and grown for 2 h at 37 °C before induction with 1 mM *i*-propyl 1-thio-β-D-galactopyranoside. After additional growth for 2 h at 37 °C, cells were harvested and disrupted by passage through a French pressure cell. A membrane fraction was isolated by centrifugation, membrane proteins were extracted with 2% DM, and permease was purified by affinity chromatography on im-

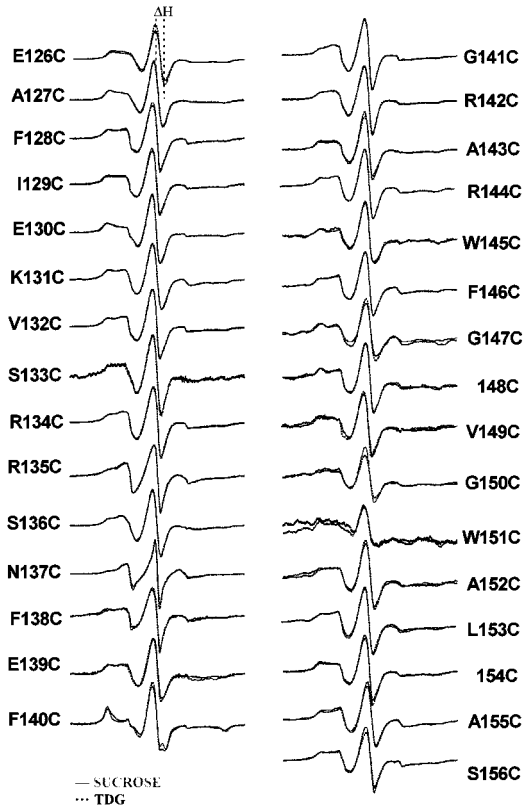

FIGURE 2: EPR spectra of nitroxide-labeled single-Cys mutants in DM. First-derivative EPR spectra of given nitroxide-labeled single-Cys lac permease mutants at positions from 126 to 156 solubilized in DM in the presence of 20 mM sucrose (gray lines) or 20 mM TDG (dotted black lines) are shown. The spectra were corrected for free spin label and scaled vertically for convenience in order to contrast differences in the presence of 20 mM sucrose or TDG. The magnetic field scan width is 100 G, and the line width of the central resonance (ΔH) is indicated on the spectrum of mutant E126C.

mobilized monomeric avidin beads as described (*15*). Purified protein was then incubated with 50 mM methanethiosulfonate spin label for 1 h at 4 °C to derivatize the Cys with the nitroxide spin label. After the column was washed with a minimum of 200 mL of column buffer [50 mM potassium phosphate (KP_i; pH 7.5)/150 mM NaCl/0.02% DM], the permease was eluted with 2 mM biotin in column buffer and concentrated with a Micro-ProDiCon membrane (Spectrum, Houston, TX) (*28*).

To prepare proteoliposomes, spin-labeled permease (5 mg/mL) in the column buffer was mixed with 1.2% octyl β-D-glucopyranoside (OG) before adding 1-palmitoyl-2-oleoylphosphatidylethanolamine and 1-palmitoyl-2-oleoylphosphatidylglycerol (3:1 mol/mol) to yield a lipid-to-protein ratio of 100. After 15 min of incubation on ice, the mixture was rapidly diluted 40-fold into 50 mM KP_i (pH 7.5). Proteoliposomes were then harvested by ultracentrifugation, resuspended in 50 mM KP_i (pH 7.5), and subjected to three cycles of freeze−thaw/sonication (*5*) prior to EPR spectroscopy.

EPR Spectroscopy. X-band EPR spectra of spin-labeled permeases were obtained at 22 °C with 10 μL of purified protein at a final concentration of ca. 50 μM in 50 mM KP_i (pH 7.5)/150 mM NaCl/0.02% DM. The samples were contained in a TPX capillary, which was placed in a Varian E-109 X-band spectrometer fitted with a loop−gap resonator (*29*, *30*). A microwave power of 2 mW and a modulation

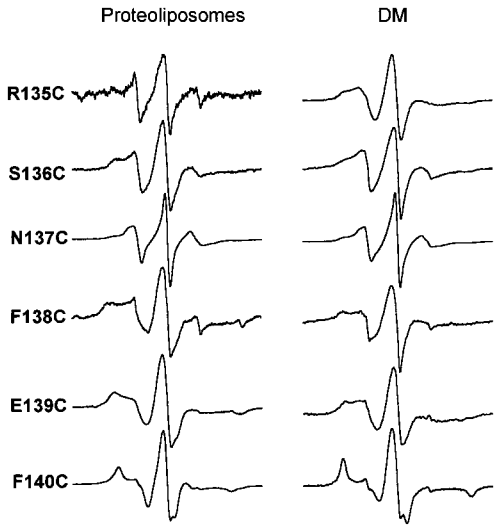

FIGURE 3: EPR spectra of nitroxide-labeled single-Cys mutants reconstituted into proteoliposomes (left) or solubilized in DM (right). First-derivative EPR spectra of nitroxide-labeled single-Cys lac permease mutants at positions from 137 to 140 after reconstitution into proteoliposomes or solubilized in DM as indicated are shown in the presence of 20 mM sucrose. The spectra were corrected for free spin label and scaled vertically for convenience. The magnetic field scan width is 100 G.

amplitude optimized for the natural line width of the individual spectra were used during recording under field-frequency lock. Signal-averaged spectra were obtained with a 100 G sweep at 40 s scan time.

Power saturation of the central resonance was carried out in the presence of O_2 in equilibrium with air or under N_2 in the absence or presence of 20 mM potassium chromium oxalate (CrOx). The parameter $P_{1/2}$, which is proportional to $1/T_{1e}T_{2e}$ (*31*),[3] is the microwave power that saturates the signal amplitude to half the value it would have reached in the absence of saturation. Spin exchange with a fast-relaxing paramagnetic species such as O_2 or CrOx results in an increase in the relaxation rate ($1/T_{1e}$) in proportion to collision frequency (*31*). The change in $P_{1/2}$ due to the presence of a paramagnetic species such as O_2 is defined as

$$\Delta P_{1/2}(O_2) = P_{1/2}(O_2) - P_{1/2}(N_2) \quad (1)$$

and is a direct measure of the collision frequency of the nitroxide with O_2. To account for the effect of T_{2e} and variations in spectrometer performance, $P_{1/2}$ is normalized to give the accessibility parameter Π, which is defined as

$$\Pi = \frac{\Delta P_{1/2}(O_2)}{P_{1/2}(\mathrm{DPPH})} \frac{\Delta H(\mathrm{DPPH})}{\Delta H} \quad (2)$$

where $P_{1/2}$(DPPH) is $P_{1/2}$ for a 2,2-diphenyl-1-picrylhydrazyl (DPPH) crystal, ΔH(DPPH) is the peak-to-peak line width of the DPPH resonance, and ΔH is the corresponding line width of the nitroxide central ($m_I = 0$) resonance (*32*).

RESULTS

EPR Spectra. EPR spectra of nitroxide-labeled permease with single-Cys replacements at positions 126−156, which

[3] T_{1e} is the spin−lattice relaxation time; T_{2e} is the transverse relaxation time.

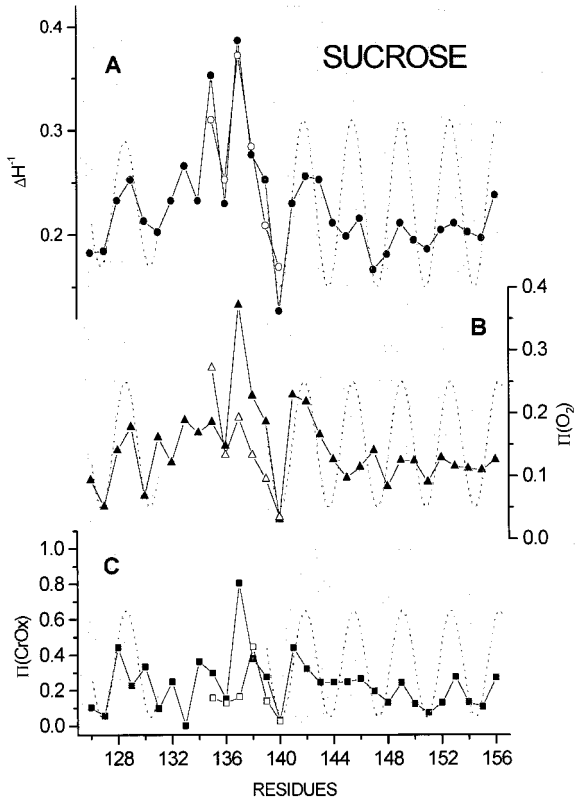

FIGURE 4: Side-chain mobility and accessibility of nitroxide side chains to O_2 or CrOx in the presence of sucrose. ΔH^{-1} (A, ●), $\Pi(O_2)$ (B, ▲), and Π(CrOx) (C, ■) versus the position of the nitroxide-labeled side chain in single-Cys mutants solubilized in DM in the presence of 20 mM sucrose. Open symbols represent data obtained with nitroxide-labeled single-Cys mutants at positions 135−140 reconstituted after reconstitution into proteoliposomes. The dotted line represents the periodicity expected for a typical α-helix. See Experimental Procedures for details.

span the C-terminal third of helix IV, helix V, and the intervening loop (loop IV/V; Figure 1), are shown in Figure 2. A component corresponding to small amounts (<5%) of free spin was subtracted, and the spectra were scaled vertically for convenience in order to contrast differences observed in the presence of sucrose, which is not a substrate for the permease, with *β*-D-galactopyranosyl 1-thio-*β*-D-galactopyranoside (TDG), a high-affinity ligand. As shown, TDG has little or no effect on the line shape of the spectra, indicating that side-chain dynamics are not significantly altered by ligand binding. However, as reflected by spectral line width and breadth (*33*), the side-chain dynamics vary widely from relatively mobile (e.g., positions 135 and 137) to highly immobilized (e.g., position 140), suggesting marked differences in tertiary contacts between this region and other domains.

Since the data shown were obtained with the permease in DM, nitroxide-labeled mutants at positions 135−140, where the side chains display the most dramatic contrast in dynamics, were also studied after reconstitution (Figure 3). Although the inverse line width of the central resonance (ΔH^{-1}) remains essentially unchanged (see Figure 4A), it is clear from the upfield and downfield regions of the spectra that nitroxides at positions 136, 138, and 139 are more immobile after reconstitution. In contrast, the spectra obtained with the other reconstituted nitroxide-labeled mutants are almost identical to those observed in DM. Thus, although the permease may be more "loosely packed" in DM, the fold is the same, a conclusion consistent with previous findings (see ref *8*). It is also noteworthy that TDG has little or no effect on the line shapes after reconstitution (data not shown).

Loop IV/V. The motional freedom[4] of a nitroxide side chain can be measured by the inverse of the peak-to-peak line width of the central resonance (ΔH^{-1}), as indicated in the spectrum for nitroxide-labeled E126C permease (Figure 2) (*33*, *34*). A plot of ΔH^{-1} versus the position of the nitroxide (Figure 4A) reveals that positions 135 and 137 display significantly higher motional freedom than the other nitroxide-labeled side chains. Increased nitroxide side-chain mobility at these positions is consistent with weak tertiary interactions. Interestingly, the other residues in the vicinity of positions 135 and 137 do not exhibit high mobility. The constraint of motion may be due to tertiary interactions with residues in other loops (e.g., a Cys residue at position 134 forms a disulfide spontaneously with certain Cys replacements in loop VIII/IX; I. Kwaw and H.R.K., unpublished observation) and/or partial embedding of the residues within the membrane. In addition, a periodicity corresponding approximately to that of an α-helix is observed from about position 140 to 156 (dotted line). Although a similar pattern is also observed from position 127 to 131, the sequence scanned is too short to draw conclusions regarding the secondary structure of transmembrane domain IV. A close examination of Figures 4 and 5 suggests that one or both of these helices may be one turn longer, ending at approximately position 134 and beginning at approximately 136, respectively. However, the resulting loop would then contain only a single residue (position 135), and it is unlikely that a single residue can bridge two antiparallel transmembrane helices. In contrast, no periodicity consistent with helical structure is observed from position 131 to 139.

Determination of the collision rates of nitroxide side chains with diffusible paramagnetic agents such as O_2 or CrOx is a complementary approach to topological mapping (*19*). The accessibility parameter (Π), proportional to the collision rate, is a direct measure of nitroxide accessibility to either water or the lipid bilayer (*35*). The pattern of accessibility to O_2 (Figure 4B) and CrOx (Figure 4C) in the sequence scanned generally mirrors that for side-chain mobility, as found in nitroxide scanning EPR studies of helix VII and loop VII/VIII (*36*), as well as helix XII (*37*), in lac permease. Thus, there is a weak but discernible periodic variation of $\Pi(O_2)$ and Π(CrOx) with positions in the region 127−131 and 140−156 compatible with helical segments. In the regions 132−138, neither $\Pi(O_2)$ nor Π(CrOx) reflects a simple helical geometry. Moreover, the relatively high values of $\Pi(O_2)$ and Π(CrOx) at position 137 clearly indicate a solvent-exposed region. Throughout the sequence 126−156, the absolute values and general pattern for $\Pi(O_2)$ are similar to those found in helix−turn−helix motifs of rhodopsin in DM micelles (*34*). Importantly, the results are consistent with the findings obtained by using amino acid deletion analysis to estimate loop−helix boundaries in this region of the permease (*18*).

[4] The term motional freedom is used in a general sense, and a change in motional freedom can arise from a change in either the rate or amplitude of motion or both.

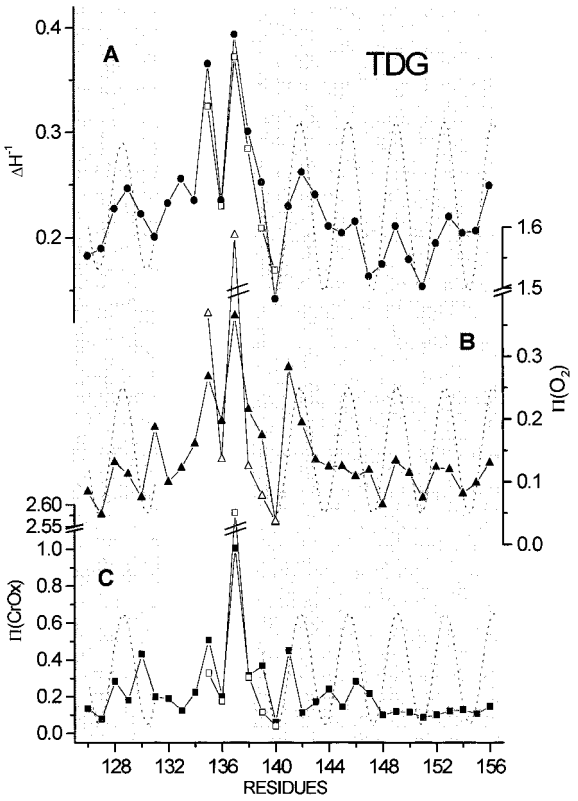

FIGURE 5: Side-chain mobility and accessibility of nitroxide side chains to O_2 or CrOx in the presence of TDG. ΔH^{-1} (A, ●), $\Pi(O_2)$ (B, ▲), and Π(CrOx) (C, ■) are shown versus the position of the nitroxide-labeled side chain in single-Cys mutants solubilized in DM in the presence of 20 mM TDG. Open symbols represent data obtained with nitroxide-labeled single-Cys mutants at positions 135−140 after reconstitution into proteoliposomes. Note the break in the *y* axis in panels B and C. The dotted line represents the periodicity expected for a typical α-helix. See Experimental Procedures for details.

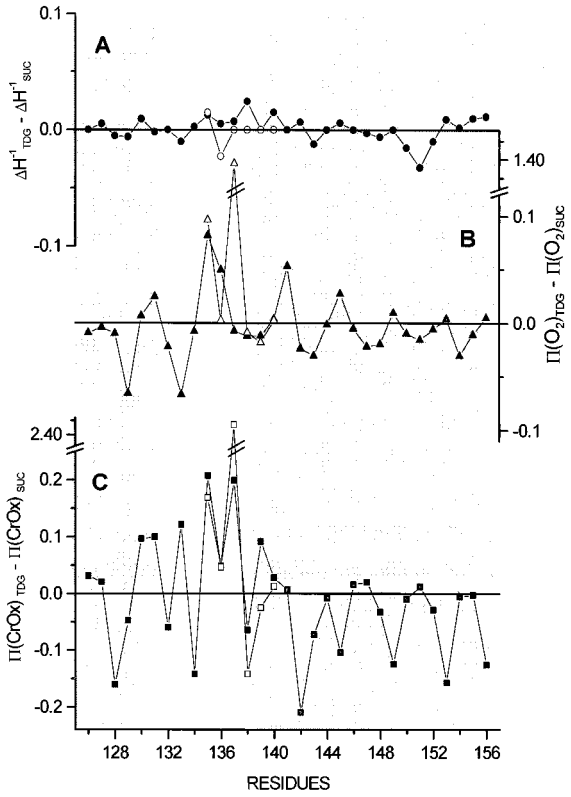

FIGURE 6: Effect of ligand on side-chain mobility and accessibility of nitroxide side chains to O_2 or CrOx. Differences are shown between values for ΔH^{-1} (A, ●), $\Pi(O_2)$ (B, ▲), and Π(CrOx) (C, ■) obtained in the presence of 20 mM sucrose, which is not a ligand for the permease (Figure 4), or 20 mM TDG, a ligand for the permease (Figure 5), versus the position of the nitroxide-labeled side chain in single-Cys mutants solubilized in DM in the presence of 20 mM TDG. Open symbols represent data obtained with nitroxide-labeled single-Cys mutants at positions 135−140 after reconstitution into proteoliposomes. Note the break in the *y* axis in panels B and C.

It is also noteworthy that the data (Figure 3) obtained with mutants 135−140 after reconstitution into proteoliposomes follow a pattern similar to that obtained in DM. However, the $\Pi(O_2)$ value of position 135 is significantly higher after reconstitution, while the Π(CrOx) value is significantly lower. In addition, $\Pi(O_2)$ values of positions 137, 138, and 139 are significantly lower after reconstitution, while the Π(CrOx) value for position 137 is much lower. Possibly, position 135 is exposed to water when the permease is solublized in DM and becomes buried in the interior of the protein after reconstitution.

Helices IV and V. For buried to completely exposed sites, respectively, in water-soluble proteins, $\Pi(O_2)$ varies from about 0.05 to 0.6. For water-exposed parts of membrane proteins, $\Pi(O_2)$ is generally less, reaching a maximum of about 0.4. For rhodopsin (*34*) and bacteriorhodopsin (*38*) in DM, the surface residues in transmembrane helices have $\Pi(O_2)$ values of 0.15−0.2, similar to those reported here. The apparent periodicity observed for side-chain mobility, as well as accessibility to O_2 and CrOx, from positions 126 to 131 and from positions 140 to 156 suggests that one face of the C-terminal third of helix IV and one face of helix V are exposed to a solvated environment, while the opposite faces are sequestered from water due to packing with other transmembrane helices in the permease (Figure 4). A periodicity that does not correspond precisely to an α-helical configuration is to be expected, as helices IV and V are probably tilted relative to each other (see ref *10*), and periodicity in the vicinity of position 144 may be interrupted because the charge pair Glu126/Arg144 is critical for local conformation (*12*). It is also interesting that the interface where Glu126 and Arg144 are located appears to be relatively hydrophobic and sequestered from water, as suggested by relatively low side-chain mobility and CrOx accessibility (<0.2) of resides on the same face of helix V as Arg144 (i.e., positions 140, 148, 151, 154, and 155).

Effect of Ligand Binding. Either in DM or after reconstitution, the mobility of the nitroxide-labeled side chains are essentially unaffected in the presence of TDG (<5% in helix V), suggesting that backbone motion remains unchanged upon ligand binding (Figures 5A and 6A; see Figures 2 and 3 in addition). With respect to O_2 accessibility (Figures 5B and 6B), little change is observed in the presence of ligand (<20% in helix V). On the other hand, CrOx accessibility (Figures 5C and 6C) exhibits a generalized flattening effect (ca. 50%), particularly from position 142 to 156, due primarily to decreased accessibility of positions 142, 146, 149, 153, and 156, suggesting that helix V may become more buried within the protein upon ligand binding. In the differential plot (Figure 6C), the residues affected from 140 to 156 appear to be located at the maxima of an oscillation with a periodicity of between 3 and 4, while a zigzag pattern

with a periodicity approximating 2 is observed from position 132 to 138. Furthermore, after reconstitution into proteoliposomes, accessibility of the nitroxide at position 137 to O_2 increases almost 8-fold, while accessibility to CrOx increases about 30-fold (Figure 6B,C; compare Figures 4A,B to Figure 5A,B, respectively). However, the relatively high accessibility of position 137 to CrOx versus O_2 indicates that position 137 remains solvent-accessible. In contrast, little change in O_2 or CrOx accessibility is induced by TDG with nitroxides at position 135, 136, or 138−140 after reconstitution.

DISCUSSION

Cytoplasmic Loop IV/V. The topology of the region subjected to nitroxide-scanning EPR here was initially predicted from hydropathy analysis (*17*) to extend from Glu126 to Arg144, with these residues at the cytoplasmic surface of the membrane. However, as indicated by a variety of site-directed approaches (*12*, *16*), Glu126 and Arg144, which are major determinants for substrate binding, are probably charge-paired and therefore likely to be located within the low dielectric of the membrane. Further studies utilizing amino acid deletion analysis (*18*) indicate that loop IV/V is much smaller than predicted, probably extending from Val132 to Phe138, and that Glu126 and Arg144 are probably located about two helical turns from the cytoplasmic ends of helices IV and V, respectively.

It has been shown with bacteriorhodopsin (*39*) and visual rhodopsin (*34*), as well as lac permease (*36*, *37*), that residues within a loop exposed to the aqueous phase exhibit a relatively high degree of side-chain mobility and a high collision frequency with polar paramagnetic species. As shown here, there is a marked increase in side-chain dynamics at positions 135 and 137 and a marked increase in CrOx accessibility at position 137, as well as an increase in O_2 accessibility. Furthermore, with the exceptions of positions 135 and 137, the other residues in the region scanned exhibit relatively low side-chain mobility and low accessibility to both O_2 and CrOx. Possibly, tertiary contacts between loop IV/V and other loops in the permease account for the findings. In any case, it is apparent that conclusions regarding the boundaries between cytoplasmic ends of helices IV or V and loop IV/V cannot be approximated by differences in accessibility of nitroxide-labeled side chains to O_2 or CrOx. On the other hand, an approximate helical periodicity is observed for side-chain mobility, as well as O_2 and CrOx accessibility, from positions 126 to 131 and from positions 140 to 156, while no distinct periodicity is observed from position 132 to 138. Therefore, more weight is given to the apparent periodicity observed in the mobility and accessibility profiles with respect to defining loop IV/V, and it seems apparent that the change in periodicity from position 132 to 138 corresponds to the region identified as loop IV/V by amino acid deletion analysis (*18*).

Helices IV and V. To observe a periodic dependence in the parameters ΔH^{-1}, $\Pi(O_2)$, and Π(CrOx) for a helical segment, the helix must have asymmetric interactions with its environment (*22*). For a putative transmembrane helix, one obvious situation is to have one face of the helix solvated by the hydrocarbon chains of the bilayer (or micelle) interior and the opposing face interacting with the remainder of the protein. In this case, ΔH^{-1} and $\Pi(O_2)$ would have local maxima that are in phase corresponding to residues facing the lipid, and Π(CrOx) would be extremely low at all positions due to the insolubility of the charged reagent in nonpolar media and the interior of a packed protein. An examination of the data shows that the periodic functions of ΔH^{-1} and $\Pi(O_2)$ are indeed in phase in the sequence 138−156. However, there is also an in-phase periodic variation of Π(CrOx) with maxima that are too high to reflect collisions with lipid exposed sites.

The EPR spectra themselves aid in resolving this apparent discrepancy. The absolute mobility of all nitroxide-labeled side chains in the sequence 138−158, reflected by the EPR line shape, is much lower than that observed for most helix surface sites in a micelle or membrane interior in other transmembrane proteins (*31*, *34*). Rather, the mobility more closely resembles sites in tertiary interaction with other parts of the protein. Together with the unusually high accessibility to CrOx, the mobility data suggest that helix V is in tertiary contact with protein on all surfaces, but an asymmetry is created by the penetration of water along one side, that facing the center of the protein. Presumably, this surface would have the weakest tertiary interactions and correspond to residues with the highest mobility and Π(CrOx) (141, 146, 149, 153, and 156).

It is difficult to draw any conclusions from $\Pi(O_2)$ in this case. Collisions appear to be low for residues on the exposed face in the micelle headgroup region and cannot be distinguished from sites buried in a loosely packed interior (*34*).

For the sequence 126−131, the situation is similar. The model suggests a lipid-solvated surface, and although limited, the EPR data are consistent with this notion. Lipid-exposed sites can be immobilized by local tertiary contact interactions for particular helix packing geometries, as shown for KcsA, the prokaryotic K^+ channel (*40*).

Based on various site-directed techniques, a helix packing model that includes tilts has been proposed (*10*). In the model, helices IV and V are next to each other, with helix V in the interior and helix IV on the periphery of the 12-helix bundle. Possibly, with the permease in DM, helices IV and V each have one face solvated in water with the interface between the helices motionally hindered and sequestered from water. Since Glu126 is ion-paired with Arg144 (*12*, *16*), it is likely that residues on the same face as Glu126 and Arg144 are located at the interface. On the basis of the data presented, helices IV and V, as well as loop IV/V, are modeled (Figure 7A). In support of the model, residues exhibiting relatively high motional freedom (>0.1) and relatively high CrOx accessibility (>0.25) occupy the same helical face (spheres). Residues at the interface between helices IV and V, which contains Glu126, Arg144, and Cys148, are relatively immobilized and less accessible to solvent. Thus, the interface between helices IV and V where the major determinants for substrate binding are located is relatively hydrophobic and sequestered from water (*12*). It is also relevant that permease with bis-His replacements at positions 126 and 144 binds Mn(II) with relatively high affinity at pH 7.5 (*16*), a finding consistent with the notion that metal-binding sites are usually centered in a shell of hydrophilic ligands surrounded by more hydrophobic side chains (*41*).

Effect of Ligand Binding. The observation that TDG has no demonstrable effect on side-chain dynamics suggests that backbone motion of helices IV and V remains the same upon

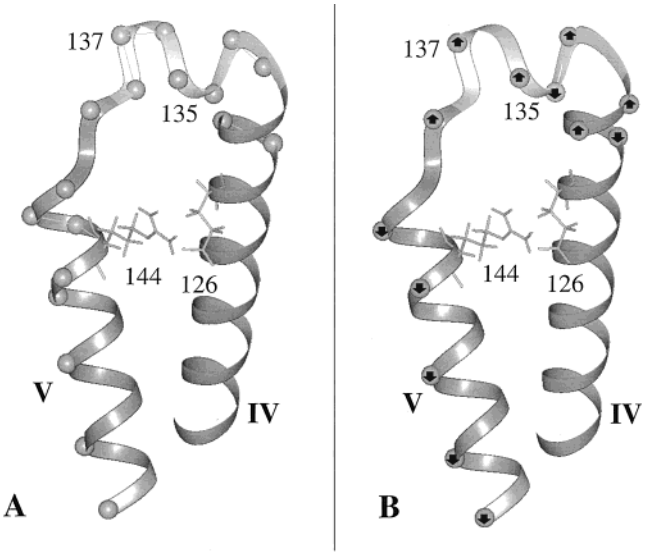

FIGURE 7: Modeling of helices IV and V and loop IV/V in lac permease. Positions 126−131 and 139−156 are presented in α-helical conformation as gray ribbons, and the positions 132−138 that represent the intervening loop are shown as a β-like structure in light gray. The Glu126/Arg144 charge pair are the only side chains shown. The spheres in panel A represent positions at which ΔH^{-1} is maximal (Figure 4A). It is also noteworthy that residues which exhibit maximal values for $\Pi(O_2)$ and Π(CrOx) occupy the same positions. The arrows in panel B indicate increased or decreased CrOx accessibility in the presence of TDG versus sucrose (Figure 5C).

ligand binding and suggests that if the helices move, they do so as rigid bodies. Rigid-body motions of a transmembrane helix can occur by rotational, translational, or tilting movements. In the case of rotational motion, one face previously accessible to solvent may become embedded in the interior of the protein and sequestered from water, while the opposing face may become more accessible to solvent. In contrast, with translational motion or tilting, the face solvated in water might remain exposed to solvent, while the face embedded in the interior of the protein might remain sequestered from solvent. The data presented here are generally inconsistent with the idea that helix V rotates upon ligand binding, as the CrOx-accessible face appears to become less accessible upon ligand binding without compensatory changes (Figure 7B). Residues that exhibit a ligand-induced change with respect to CrOx accessibility occupy the surface opposite the interface between helices IV and V [downward or upward arrows represent decreased or increased Π(CrOx) accessibility, respectively]. Therefore, it appears that helix V undergoes translational motion and/or a change in tilt, a contention consistent with ligand-binding effects on Cys cross-linking between helices IV and V (C. D. Wolin and H.R.K., unpublished observations).

Nitroxides at positions 136, 138, or 139 exhibit significant decreases in mobility after reconstitution relative to DM, while the nitroxide spectra of permease labeled at position 137 or 140 remain unchanged (Figure 3), indicating that the permease may be more loosely packed in the detergent. Although most of the data presented here were obtained with permease solubilized in DM, it should be emphasized that a variety of approaches (*15*, *16*, *42*−*45*) are in agreement with the contention that the permease retains near-native structure in DM. Moreover, except for E126C and R144C permease, most of the other 29 Cys-replacement mutants used in this study display good transport activity (*9*, *23*).

ACKNOWLEDGMENT

We are grateful to Cindy Weitzman and Stathis Frillingos for preparing the single-Cys mutants and to J. Sun and D. S. Malashock for inserting the biotin acceptor domain.

REFERENCES

1. Müller-Hill, B. (1996) *The lac Operon: A Short History of a Genetic Paradigm*, Walter de Gruyter, Berlin and New York.
2. Kaback, H. R. (1976) *J. Cell. Physiol. 89*, 575−593.
3. Kaback, H. R. (1983) *J. Membr. Biol. 76*, 95−112.
4. Kaback, H. R. (1986) in *Physiology of Membrane Disorders* (Andreoli, T. E., Hoffman, J. F., Fanestil, D. D., and Schultz, S. G., Eds.) pp 387−408, Plenum, New York.
5. Viitanen, P., Newman, M. J., Foster, D. L., Wilson, T. H., and Kaback, H. R. (1986) *Methods Enzymol. 125*, 429−452.
6. Sahin-Tóth, M., Lawrence, M. C., and Kaback, H. R. (1994) *Proc. Natl. Acad. Sci. U.S.A. 91*, 5421−5425.
7. Kaback, H. R. (1996) in *Handbook of Biological Physics: Transport Processes in Eukaryotic and Prokaryotic Organisms* (Konings, W. N., Kaback, H. R., and Lolkema, J. S., Eds.) pp 203−227, Elsevier, Amsterdam.
8. Kaback, H. R., and Wu, J. (1997) *Q. Rev. Biophys. 30*, 333−364.
9. Frillingos, S., Sahin-Tóth, M., Wu, J., and Kaback, H. R. (1998) *FASEB J. 12*, 1281−1299.
10. Kaback, H. R., and Wu, J. (1999) *Acc. Chem. Res. 32*, 805−813.
11. Frillingos, S., Gonzalez, A., and Kaback, H. R. (1997) *Biochemistry 36*, 14284−14290.
12. Venkatesan, P., and Kaback, H. R. (1998) *Proc. Natl. Acad. Sci. U.S.A. 95*, 9802−9807.
13. Sahin-Tóth, M., le Coutre, J., Kharabi, D., le Maire, G., Lee, J. C., and Kaback, H. R. (1999) *Biochemistry 38*, 813−819.
14. Jung, H., Jung, K., and Kaback, H. R. (1994) *Biochemistry 33*, 12160−12165.
15. Wu, J., and Kaback, H. R. (1994) *Biochemistry 33*, 12166−12171.
16. Zhao, M., Zen, K.-C., Hubbell, W., and Kaback, H. R. (1999) *Biochemistry 38*, 7407−7412.
17. Foster, D. L., Boublik, M., and Kaback, H. R. (1983) *J. Biol. Chem. 258*, 31−34.
18. Wolin, C., and Kaback, H. R. (1999) *Biochemistry 38*, 8590−8597.
19. Hubbell, W. L., and Altenbach, C. (1994) in *Membrane Protein Structure* (White, S. H., Ed.) pp 224−248, Oxford University Press, New York.
20. Hubbell, W. L., and Altenbach, C. (1994) *Curr. Opin. Struct. Biol. 4*, 566−573.
21. Hubbell, W. L., Mchaourab, H. A., Altenbach, C., and Lietzow, M. A. (1996) *Structure 4*, 779−783.
22. Hubbell, W. L., Gross, A., Langen, R., and Lietzow, M. A. (1998) *Curr. Op. Struct. Biol. 8*, 649−656.
23. Weitzman, C., and Kaback, H. R. (1995) *Biochemistry 4*, 2310−2318.
24. Frillingos, S., Sun, J., Gonzalez, A., and Kaback, H. R. (1997) *Biochemistry 36*, 269−273.
25. Consler, T. G., Persson, B. L., Jung, H., Zen, K. H., Jung, K., Prive, G. G., Verner, G. E., and Kaback, H. R. (1993) *Proc. Natl. Acad. Sci. U.S.A. 90*, 6934−6938.
26. Sanger, F., Nicklen, S., and Coulson, A. R. (1977) *Proc. Natl. Acad. Sci. U.S.A. 74*, 5463−5467.
27. Hattori, M., and Sakaki, Y. (1986) *Anal. Biochem. 152*, 1291−1297.
28. Voss, J., Hubbell, W. L., and Kaback, H. R. (1995) *Proc. Natl. Acad. Sci. U.S.A. 92*, 12300−12303.
29. Froncisz, W., and Hyde, J. S. (1982) *J. Magn. Reson. 47*, 515−521.
30. Hubbell, W. L., Froncisz, W., and Hyde, J. S. (1987) *Rev. Sci. Instrum. 58*, 1879−1886.

31. Altenbach, C., Flitsch, S. L., Khorana, H. G., and Hubbell, W. L. (1989) *Biochemistry 28*, 7806−7812.
32. Farahbakhsh, Z. T., Altenbach, C., and Hubbell, W. L. (1992) *Photochem. Photobiol. 56*, 1019−1033.
33. Machaourab, H., Lietzow, M. A., Hideg, K., and Hubbell, W. L. (1996) *Biochemistry 35*, 7692−7704.
34. Altenbach, C., Yang, K., Farrens, D., Khorana, H. G., and Hubbell, W. L. (1996) *Biochemistry 35*, 12470−12478.
35. Resek, J. F., Farahbakhsh, Z. T., Hubbell, W. L., and Khorana, H. G. (1993) *Biochemistry 32*, 12025−12032.
36. Voss, J., Hubbell, W. L., Hernandez, J., and Kaback, H. R. (1997) *Biochemistry 36*, 15055−15061.
37. Voss, J., He, M., Hubbell, W., and Kaback, H. R. (1996) *Biochemistry 35*, 12915−12918.
38. Greenhalgh, D. A., Altenbach, C., Hubbell, W. L., and Khorana, H. G. (1991) *Proc. Natl. Acad. Sci. U.S.A. 88*, 8626−8630.
39. Henderson, R., Baldwin, J. M., Ceska, T. A., Zemlin, F., Beckmann, E., and Downing, K. H. (1990) *J. Mol. Biol. 213*, 899−929.
40. Gross, A., Columbus, L., Hideg, K., Altenbach, C., and Hubbell, W. L. (1999) *Biochemistry 38*, 10324−10335.
41. Yamashita, M. M., L., W., Eisenman, G., and Eisenberg, D. (1990) *Proc. Natl. Acad. Sci. U.S.A. 87*, 5648−5653.
42. Jung, K., Voss, J., He, M., Hubbell, W. L., and Kaback, H. R. (1995) *Biochemistry 34*, 6272−6277.
43. He, M. M., Voss, J., Hubbell, W. L., and Kaback, H. R. (1995) *Biochemistry 34*, 15667−15670.
44. He, M. M., Voss, J., Hubbell, W. L., and Kaback, H. R. (1995) *Biochemistry 34*, 15661−15666.
45. Sun, J., Li, J., Carrasco, N., and Kaback, H. R. (1997) *Biochemistry 36*, 274−280.

BI991754X